Thin Solid Films 774 (2023) 139844

Contents lists available at ScienceDirect

Thin Solid Films

journal homepage: www.elsevier.com/locate/tsf

Characteristics of thin Sb_2Se_3 films obtained by the chemical molecular beam deposition method for thin-film solar cells

T.M. Razykov [a], K.M. Kuchkarov [a,*], M.S. Tivanov [b,*], D.S. Bayko [b], L.S. Lyashenko [b], B. A. Ergashev [a], A. Mavlonov [c], A.N. Olimov [a], R. Khurramov [a], D.Z. Isakov [a], M. Pirimmatov [a]

[a] Physical-Technical Institute, Uzbekistan Academy of Sciences, Chingiz Aitmatov St., 2, Tashkent 100084, Uzbekistan
[b] Faculty of Physics, Belarusian State University, Minsk 220030, Belarus
[c] Research Organization of Science and Technology, Ritsumeikan University, 1-1-1 Nojihigashi, Kusatsu, Shiga 525-8577, Japan

ARTICLE INFO

Keywords:
Antimony triselenide
Chemical molecular beam deposition
Structure
Morphology

ABSTRACT

Sb_2Se_3 films were obtained by chemical molecular beam deposition on soda-lime glass substrates. As a source material, 99.999% purity semiconductor Sb_2Se_3 pieces were used. Their evaporation and the substrate temperature were maintained at 830 °C÷1000 °C and 500 °C, respectively. Using scanning electron microscopy, X-ray diffraction analysis, and Raman scattering, the influence of the temperature of the source of the binary compound Sb_2Se_3 on the chemical composition, morphology, and structure of the synthesized films of Sb_2Se_3 films was studied. It is observed that the films have a crystalline (orthorhombic) structure with compactly located crystallites having the form of rods with an average size: $l = 5 \div 10$ μm (length) and $d = 1 \div 2$ μm (diameter). An analysis of the dependency functions $(\alpha h\nu)^2 = f(h\nu)$ showed that the Sb_2Se_3 films obtained at temperatures T_{source}=900 °C and T_{source}=840 °C have direct transitions with an optical band gap E_g=1.04 eV and E_g=1.12 eV, respectively. The electrical conductivity of the films, changed within $1.03 \cdot 10^{-5} \div 4.13 \cdot 10^{-5}$ $(Om \cdot cm)^{-1}$ depending on the ratio of Sb/Se atomic concentration.

1. Introduction

Today, world researchers pay special attention to the use of new Sb_2Se_3, Sb_2S_3 and $Sb_2(Se,S)_3$ materials [1,2] as an absorbing layer for solar cells. This is because the physical properties (p-type conductivity, tunable band gap E_g=1.1–1.8 eV, high absorption coefficient $\alpha > 10^5$ cm^{-1}, low melting temperature and high partial pressure) of these materials are very close to the properties of $Cu(In,Ga)(Se,S)_2$ [3]. In addition, the elements included in these materials have a relatively low cost (prevalence in nature), stability under external influences and non-toxicity. This will make it possible to produce environmentally friendly and efficient solar modules, as well as open up ways for their widespread production in an industrial scale.

In recent years, the structure and properties of Sb_2Se_3 thin films have been intensively studied in order to determine the possibility of their application in the manufacture of solar cells [4–7]. The films synthesized by various methods (rapid thermal evaporation in vacuum, magnetron sputtering, chemical vapor deposition, etc.) consist mainly of the Sb_2Se_3 phase (JCPDS-00–015–0861) with a rhombic crystal lattice (space group P_{nma}, no. 62) [8–18], in which each antimony atom and each selenium atom are bound by a strong covalent bond with three selenium and antimony atoms, respectively, which are then held together in the crystal by Van der Waals forces [3]. Such a structure causes anisotropic optical and electrical properties. The surface morphology of the films also differs greatly depending on the conditions (substrate and source temperatures) and the synthesis method [19,20]. It is mentioned in a number of works that films with crystal orientation (*hk*1) are more efficient for application in photovoltaics, while (*hk*0) is less efficient [21, 22]. Therefore, by varying the synthesis conditions and methods, it is possible to obtain highly efficient Sb_2Se_3 thin films with the texture required for solar cells.

Previously, we investigated the structural and morphological properties of Sb_2Se_3 films obtained by chemical molecular beam deposition (CMBD) from powders of the binary compound Sb_2Se_3 at various substrate temperatures. The results showed that all the films were enriched in antimony and had an orthorhombic structure with predominant (120) and (221) orientations with the film crystallite sizes were 200÷300 nm [23].

* Corresponding authors.
E-mail addresses: k.kuchkarov@mail.ru (K.M. Kuchkarov), tivanov@bsu.by (M.S. Tivanov).

https://doi.org/10.1016/j.tsf.2023.139844
Received 19 September 2022; Received in revised form 11 April 2023; Accepted 11 April 2023
Available online 12 April 2023

In this work, the effect of the temperature of the source of the Sb_2Se_3 binary compound on the chemical composition, morphology and structure of Sb_2Se_3 films obtained by CMBD at a substrate temperature of 500 °C was studied.

2. Experimental

Sb_2Se_3 thin films were deposited by CMBD, schematic representation shown in Fig. 1. The cheap and economical CMBD method has a number of advantages as follows:

- the deposition process is carried out in an atmospheric pressure gas flow, expensive vacuum or other equipment is not required;
- the extraction process is controlled at the molecular level (10^{10}–10^{14} cm^{-2}), which allows precise control of the thin film composition;
- the growth rate varies over a wide area (10÷10^4 Å/s);
- thin films can be grown on large surfaces;
- doping of thin films is carried out during the deposition process;
- toxic gasses are not used.

Before the CMBD deposition of Sb_2Se_3 films, the substrates were chemically cleaned with a soapy solution and in ultrasonic bath substrates were washed in solutions of acetic acid, in distilled water, in ethanol, respectively. Then cleaned substrates were dried in flow of nitrogen gas. The process of obtaining Sb_2Se_3 films by the CMBD method was as follows. The granules of the binary compound Sb_2Se_3 (purity 99.999%; Chemsavers) were used as a source material. The pieces of Sb_2Se_3 were placed into containers. Next, the system was brought into working condition and purged with hydrogen to remove atmospheric and polluting gasses. The outer furnace of the reaction chamber was then turned on. The heating level is determined by the set deposition temperatures, which are controlled by thermocouples. Upon reaching the required substrate temperature, the furnaces for individual heating of the Sb_2Se_3 binary compound were turned on and brought to the required evaporation temperatures. The evaporation temperature range of the film-growth binary compound pellets was from 830 to 1000 °C, and the substrate temperature was maintained at 500 °C. The hydrogen carrier gas flow was -20 cm^3/min. The deposition process was carried out for 30 min. Soda-lime glasses were used as substrates. The dimensions of the samples are 2.0 × 2.0 cm^2. The partial pressures of Sb_2Se_3 in the vapor phase were changed by controlling the source temperatures during the deposition process to obtain Sb_2Se_3 films of various compositions.

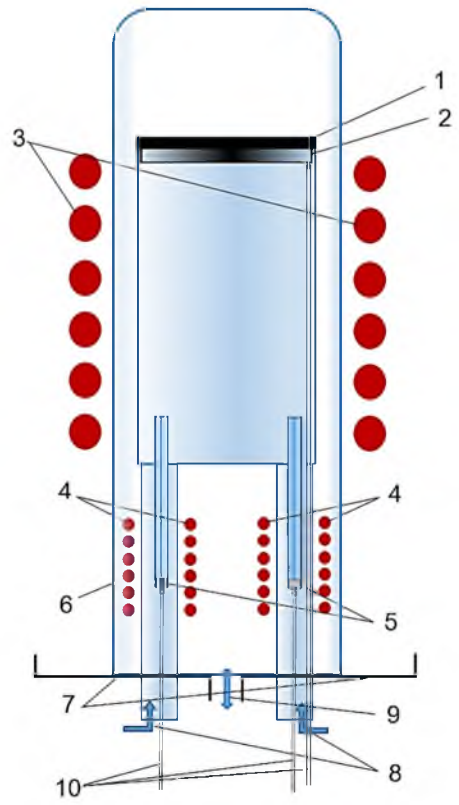

Fig. 1. Schematic representation of the CMBD method for obtaining Sb_xSe_y thin films. 1, 2 – substrate and holder, 3 – substrate heater, 4 – source heaters, 5 – crucibles of evaporated components, 6 – reactor cap, 7 – flange, 8 – gas inlet, 9 – gas outlet, 10 – thermocouples.

The elemental (chemical) composition of the synthesized Sb_2Se_3 films was determined by X-ray spectral microanalysis (XSMA) using an Aztec Energy Advanced X-Max 80 energy-dispersive nitrogen-free spectrometer. The surface morphology was studied by scanning electron microscopy (SEM) using a LEO-1455 VP microscope (Carl Zeiss) with accelerating voltage of 20 kV and by atomic force microscopy (AFM) using a Solver Nano (NT-MDT) microscope in the semi-contact mode with a cantilever with a tip radius of 10 nm at a resonant frequency of 236 kHz. X-ray diffraction patterns were taken on a Rigaku Ultima IV high-resolution diffractometer in the grazing incidence diffraction geometry (GIXD) at 1 ° of incident X-rays with CuK_α radiation source (λ=1.5418 Å) scanned in the angle range 2θ=10°÷60°. Phase identification was carried out by comparing the experimentally found interplanar distances with tabulated values from the database of the Joint Committee on Powder Diffraction Standard (JCPDS). The Raman spectra were measured at room temperature using a Nanofinder HE (LOTIS TII) confocal spectrometer. A solid-state laser with a wavelength of 532 nm was used. Laser radiation with a power of 60 μW was focused on the surface of the samples to a region about 0.7 μm in diameter. The spectral resolution was no worse than 2.5 cm^{-1}.

The crystal lattice parameters (a, b, c) of the phases that the films contain were determined using Rigaku Data Analysis Software PDXL2 (version 2.8.4.0) by the formulas:

- for Sb_2Se_3 belonging to the rhombic syngony

$$\frac{1}{d_{hkl}^2} = \left(\frac{h^2}{a^2} + \frac{k^2}{b^2} + \frac{l^2}{c^2}\right), \quad (1)$$

- for Sb belonging to the trigonal (rhombohedral) syngony

$$\frac{1}{d_{hkl}^2} = \frac{(h^2 + k^2 + l^2)\sin^2\phi + 2(hk + kl + hl)(\cos^2\phi - \cos\phi)}{a^2(1 - 3\cos^2\phi + 2\cos^3\phi)}, \quad (2)$$

where ϕ is the angle between the base vectors.

The transmission and specular reflection spectra of the films were obtained using Photon RT (Essent Optics) spectrophotometer in the wavelength range of 400÷3000 nm with spectral resolution better than 5 nm using unpolarized light at room temperature.

3. Results and discussion

The chemical composition of the elements of the obtained Sb_2Se_3 films is presented in Table 1. As can be seen from this table, it follows

Table 1
Atomic percentages determined through XSMA of Sb_2Se_3 thin films deposited at different source temperatures.

T_{source}, °C		830	840	900	975	980	1000
C, at.%	Sb	42	40	47	41	47	45
	Se	58	60	53	59	53	55

that the synthesized films consist of antimony and selenium, while the content of Sb varies in the range of 40÷47 at.%, the rest is Se, i.e. the ratio of these components is close to 2:3, without a clear dependence on the source temperature. In accordance with the state diagram of the Sb-Se system [24], the presence of the Sb_2Se_3 phase can be expected in the films.

On multilayer maps of the distribution of elements in Sb_2Se_3 films, one can see a fairly uniform distribution of the composition elements (Fig. 2).

Morphology studies of the film surface were carried out by SEM (Fig. 3) in secondary electrons mode. It was found that their structure consists mainly of randomly located rods, which, depending on T_{source}, have different characteristics such as inclinations to the substrate, variation in size, the density of their arrangement, the presence or absence of microcavities and microcracks. A relatively similar morphology is found for films obtained at T_{source}=830 °C and 840 °C (Fig. 3a, b), the surfaces of the compactly grown rods, with a diameter of $d = 1 \div 2$ μm and a length of $l = 5 \div 10$ μm, fully covered the substrate surface. At the same time, in the synthesized films at T_{source}=830 °C, the growth of rods inclined relative to the substrate is observed, and at T_{source}=840 °C, the preferred growth of microcrystallites is observed parallel to it. From the analysis of SEM images of the film cross-sections, it can be seen that the inclination of the rods for T_{source} =830 °C and T_{source}=840 °C are about 0°÷40°and 0°÷10°, respectively (Fig. 4a, b), even both films had the similar thickness of 1÷2 μm. It should be noted that the surface of these films visualizes microcracks, the formation of which is possibly due to the relaxation of microstresses via an increase in their level as a result of the competition of microcrystals to grow in different directions in the lower layer. The film obtained at T_{source}=900 °C (Fig. 3c) is an array of randomly arranged rods: small rods with $d = 1 \div 2$ μm, $l = 5$ μm and large rods with $d = 3$ μm, $l = 15 \div 20$ μm. In this case, the rods are inclined to the substrate in the range of angles from 0° to 60°, however, the vast majority have an inclination angle of 40÷45° (Fig. 4c), and the growth of microcrystals parallel or perpendicular to the substrate is suppressed. It should be noted that the decrease in compactness in their arrangement led to the absence of microcracks. The maximum film thickness for samples of this series is about 2.5 μm.

The morphologies of the films obtained at T_{source}=975 °C and T_{source}=980 °C (Fig. 3d, e) are practically indistinguishable from each other, they have a sharply different film surface in comparison with others. The size of the crystallites decreases sharply and is about 3 μm long and about 1 μm in diameter. The inclination of the rods is from 0° to 35°, the thickness of the films is 1 μm (Fig. 4d, e).

The film obtained at T_{source}=1000 °C (Fig. 3f) differs significantly from all samples in terms of surface morphology by its low compactness – the SiO_2 substrate is strongly visible dark areas on the multilayer map of the distribution of chemical elements (Fig. 3d); crystallite sizes: $d = 0.5 \div 1$ μm and $l = 2 \div 4$ μm. The average film thickness is about 1 μm (Fig. 4f).

Fig. 5. show typical AFM images of various parts of the film surface. Studies conducted using AFM showed that the films have a highly developed surface relief. The value of the average surface roughness S_a is quite high and is about 0.3÷0.7 μm (Table 2).

GIXD patterns of the studied films are shown in Fig. 6. Analyzing the literature data and the data obtained from the phase diagram of the Sb-Se system, as well as the qualitative phase analysis performed using the JCPDS database (card No. 00–015–0861 and No.01–085–1322), it was found that the films grown at different source temperatures consist predominantly of Sb_2Se_3 (blue lines), and Sb to a lesser extent (red lines), respectively. The film obtained at T_{source}=830 °C mainly consists of the Sb_2Se_3 phase, since the Sb reflections are weakly visualized in the corresponding diffraction pattern and their total integrated intensity is insignificant. For the rest of the films, an increase in the total integrated intensity of the Sb lines is observed, which indicates a certain increase in its volume fraction with increasing source temperature. In accordance with the JCPDS file, the Sb_2Se_3 phase has a rhombic crystal structure (space group P_{nma}, no.62) with lattice constants $a = 1.1630$ nm, $b = 1.1780$ nm, $c = 0.3985$ nm, and a primitive cell volume of 0.524 nm^3.

The unit cell parameters of the Sb_2Se_3 samples calculated using formulas (1) and (2) are shown in Fig. 7 and agree with the lattice constants corresponding to the JCPDS card (No. 00–015–0861), which is an additional indication for the high crystallinity of the synthesized films.

Fig. 8 depicts the Raman spectra of Sb_2Se_3 films synthesized at different temperatures, observed Raman modes are shown in the Table 3. All samples are characterized by the presence of peaks corresponding to antimony selenide (80, 151, 185, 189, 210 cm^{-1}), various phases of selenium (102, 129, 234–237, 250 cm^{-1}) and antimony oxide (118–123, 140, 189, 255 cm^{-1}) [25–30]. Difficulties in finding the presence of the pure antimony phase are created by the fact that the peak of 150 cm^{-1} is characteristic of both antimony and antimony selenide, but the presence of a peak at 110 cm^{-1} suggests that pure antimony is present in films synthesized at T_{source}=840, 900, 980 and 1000 °C. [25,26]. This contradicts the data of X-ray diffraction analysis, according to which the antimony phase is indicated only in films with T_{source}=980 and 1000 °C. This discrepancy is explained by the fact that X-rays provide information about the phase composition of the sample volume, and laser radiation is strongly absorbed by the film and does not penetrate deep into the material. According to our calculations, taking into account the characteristics of the optical properties of the films, the penetration depth of laser radiation is less than thirty nanometers.

Fig. 9a, b shows the optical transmission (T) and reflection (R) spectra of Sb_2Se_3 films deposited at T_{source}=900 °C and 840 °C. Using the optical transmission and reflection data, the absorption coefficient (α) of the films was determined by the following equation:

$$\alpha = \frac{1}{d}\ln\left(\frac{\sqrt{(1-R)^4 + 4T^2R^2} - (1-R)^2}{2TR^2}\right), \quad (3)$$

where d is the thickness of the films.

Assuming that the band-to-band transition is direct allowed, the optical band gap energy (E_g) of the layers was evaluated by the Tauc relation [31]:

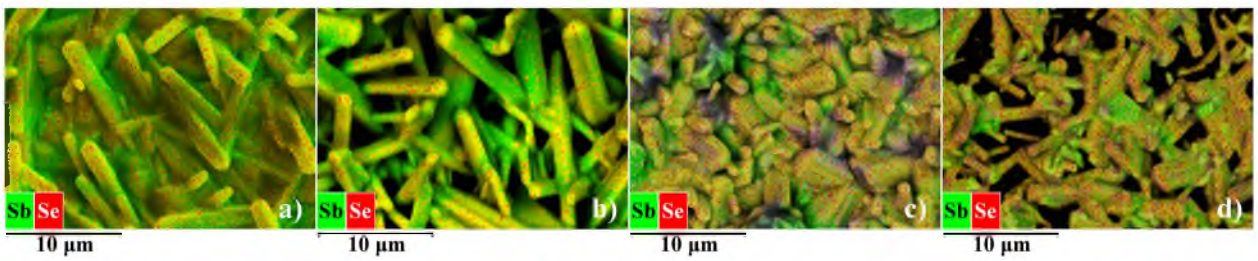

Fig. 2. Multilayer distribution maps of chemical elements in Sb_2Se_3 films synthesized at T_{source} (°C): 830 (a), 900 (b), 980 (c), 1000 (d).

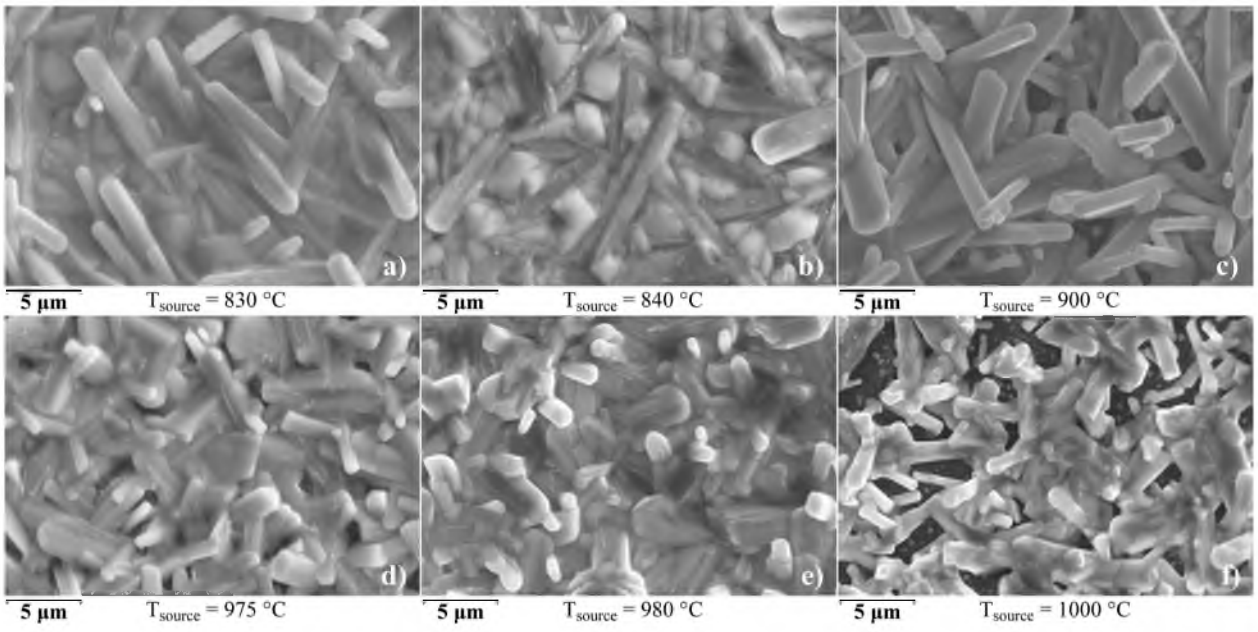

Fig. 3. Surface morphology of thin Sb_2Se_3 films synthesized at different Sb_2Se_3 source temperatures, obtained by SEM.

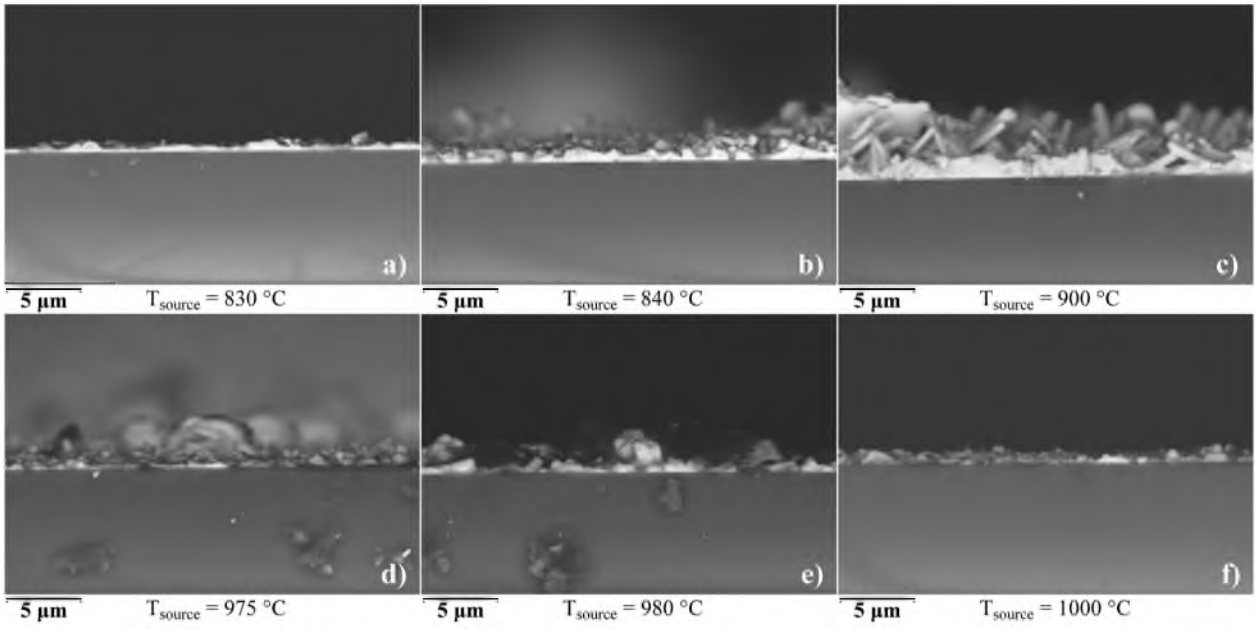

Fig. 4. Cross-section morphology of thin Sb_2Se_3 films synthesized at different Sb_2Se_3 source temperatures, obtained by SEM.

$$(\alpha h\nu)^2 = A(h\nu - E_g), \quad (4)$$

where $h\nu$ is the incident photon energy and A is a constant. The $(\alpha h\nu)^2$ versus $h\nu$ plots of Sb_2Se_3 films are shown in the Fig. 9c, from which the band gap energy can be evaluated by extrapolating the linear portion of the plots onto the energy axis. The determined E_g values of Sb_2Se_3 films were 1.04 and 1.12 at different T_{source} values. The decrease in band gap energy of the films is due to variation in composition leading to the appearance of different phases and improvement in crystalline quality of the films [32,33].

The electrical conductivity of Sb_2Se_3 films enriched in antimony and close to the stoichiometric composition was determined from the temperature dependence of the electrical conductivity. The electrical parameters of the Sb_2Se_3 films are given in Table 4. As can be seen from Table 4, with an increase in the ratio of the atomic concentration Sb/Se ($0.66 \leq Sb/Se \leq 0.88$), the electrical conductivity of the Sb_2Se_3 films changed in a narrow interval.

A change in the conduction type of charge carriers was also observed depending on the ratio of the Sb/Se atomic concentration. The samples had n-type conductivity in the range of compositions $0.81 \leq Sb/Se \leq 0.88$, and at $0.66 \leq Sb/Se \leq 0.72$ p-type. At the same time, an inversion of the conduction type was found at $0.72 < Sb/Se < 0.81$, which is close to the stoichiometric composition of Sb_2Se_3.

4. Conclusions

The structural and morphological properties of Sb_2Se_3 thin films, synthesized via CMBD at different source temperatures of the Sb_2Se_3

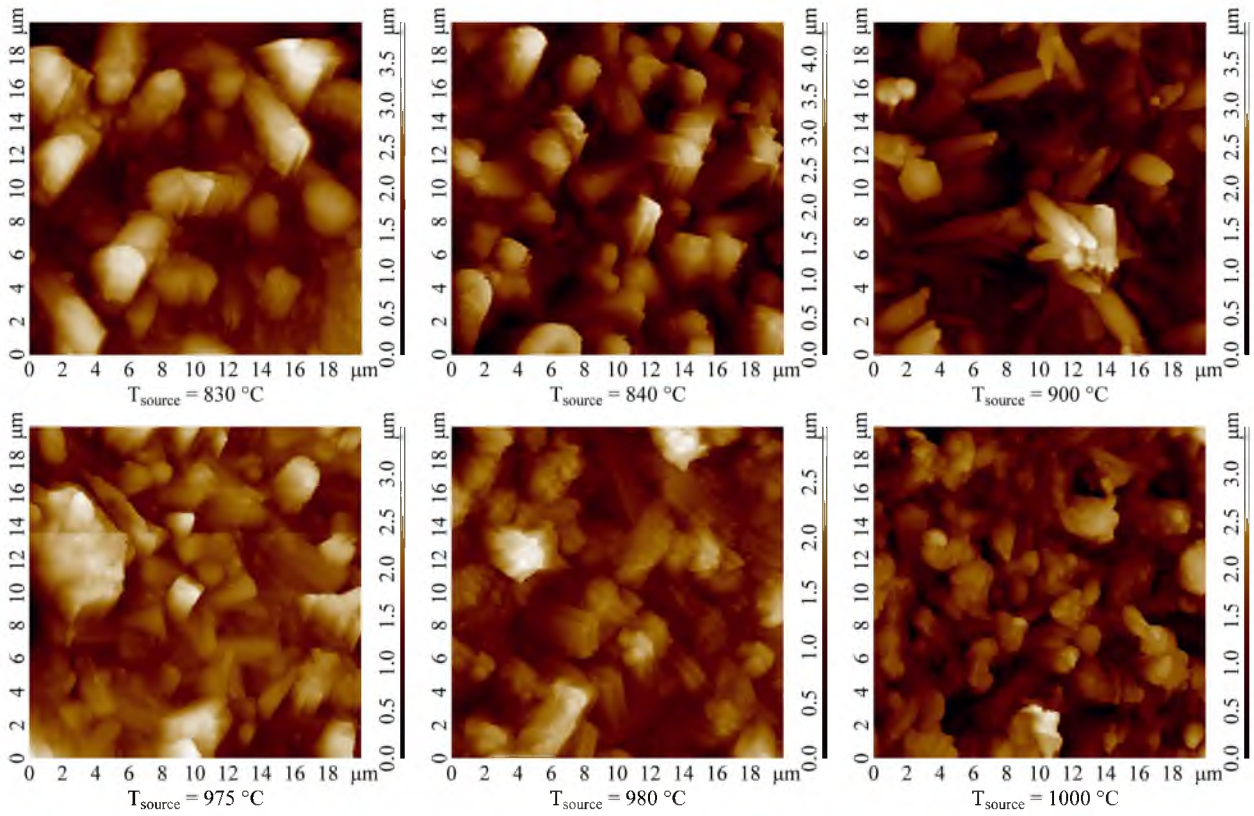

Fig. 5. 2D topography obtained on an AFM of the surface of Sb_2Se_3 films synthesized at different temperatures of the Sb_2Se_3 source.

Table 2
Surface roughness parameters of thin Sb_2Se_3 films synthesized at different temperatures of the Sb_2Se_3 source.

T_{source}	830 °C	840 °C	900 °C	975 °C	980 °C	1000 °C
Average roughness Sa, μm	0.49	0.62	0.79	0.37	0.54	0.42
RMS roughness Sq, μm	0.62	0.76	0.97	0.48	0.67	0.53
Ssk asymmetry	0.39	0.55	0.33	0.79	0.64	0.41
Ska kurtosis	3.48	2.83	2.90	3.95	3.24	3.29

binary compound, were studied. The conducted studies allow us to draw the following conclusions. Results X-ray diffraction analysis showed that the synthesized films at different source temperatures consist of both the Sb_2Se_3 phase and the Sb phase, with the volume fraction of Sb increasing with increasing source temperature, which is characterized by a rhombic crystal lattice (space group P_{nma}, No. 62, JCPDS-00–015–0861) and has a high crystallinity. The SEM images showed that the Sb_2Se_3 films obtained at different source temperatures consist mainly of randomly located rods that differ in size (length l varies in the range of 2÷20 μm, diameter d is 0.5÷3 μm) and the rods are inclined to the substrate in the range of angles from 0° to 60°. The AFM images showed that the Sb_2Se_3 films are characterized by a developed relief with an average surface roughness S_a=0.4÷0.8 μm. The results of Raman spectroscopy confirmed the formation of the main phase Sb_2Se_3 in the films, however, for the film obtained at T_{source}=840 °C and 975 °C, the presence of a side phase, trigonal Se, was detected. Overall, maximum source temperature to obtain Sb_2Se_3 was found to be <900 °C, further increasing the source temperature resulted to increase the Sb fraction and reduced uniformity of the film surface. An analysis of the dependency functions $(\alpha h\nu)^2 = f(h\nu)$ showed that for the obtained Sb_2Se_3 films in the temperature range T_{source}=900 °C and T_{source}=840 °C they

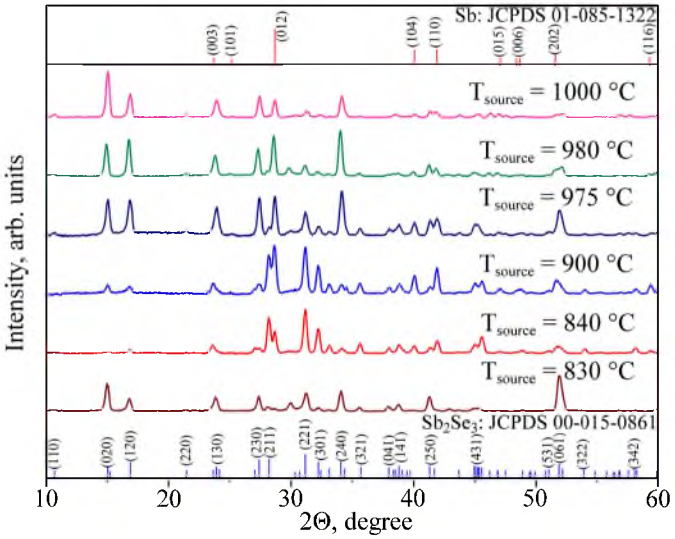

Fig. 6. GIXD patterns of Sb_2Se_3 films synthesized at different temperatures of the Sb_2Se_3 source.

have direct transitions with an optical band gap E_g=1.04 eV and E_g=1.12 eV, respectively. The results of measuring the electrical properties of the films showed that with a decrease in the ratio of the atomic concentration of Sb/Se, the electrical conductivity of the Sb_2Se_3 films changed insignificantly, and the samples also had p-type conductivity in the composition range 0.66≤Sb/Se≤0.72 and 0.81<Sb/Se≤0.88 which corresponds to n-type conductivity.

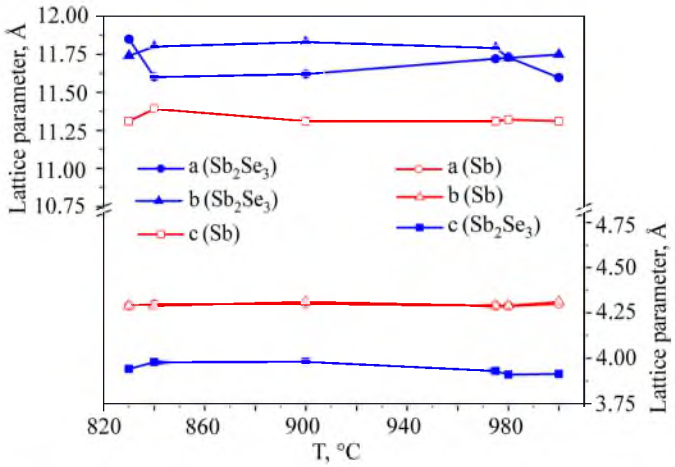

Fig. 7. Crystal lattice parameters of Sb_2Se_3 and Sb films synthesized at different temperatures of the source Sb_2Se_3.

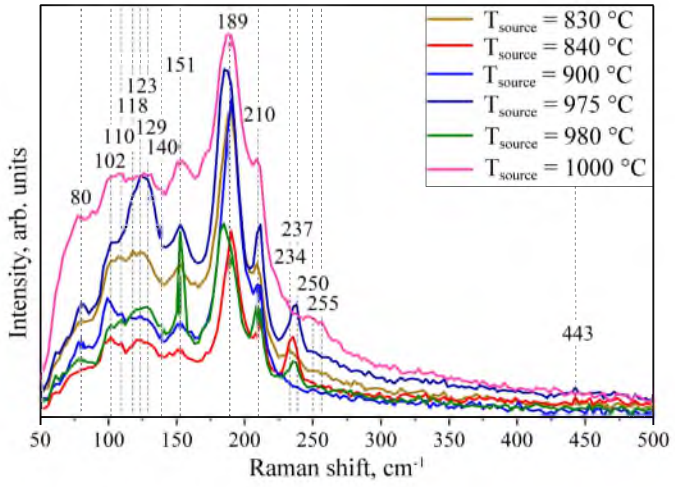

Fig. 8. Raman spectra of Sb_2Se_3 films synthesized at different temperatures of the Sb_2Se_3 source.

CRediT authorship contribution statement

T.M. Razykov: Conceptualization, Methodology, Supervision, Investigation, Writing – review & editing. **K.M. Kuchkarov:** Resources, Data curation, Formal analysis, Conceptualization, Methodology, Funding acquisition, Writing – original draft, Investigation, Writing – review & editing. **M.S. Tivanov:** Resources, Data curation, Formal analysis, Writing – original draft, Investigation, Conceptualization, Methodology, Writing – review & editing. **D.S. Bayko:** Formal analysis, Investigation, Conceptualization, Methodology, Writing – review & editing. **L.S. Lyashenko:** Formal analysis, Investigation, Conceptualization, Methodology, Writing – review & editing. **B.A. Ergashev:** Resources, Data curation, Formal analysis, Investigation, Conceptualization, Methodology, Writing – review & editing. **A. Mavlonov:** Resources, Data curation, Formal analysis, Visualization, Writing – original draft, Funding acquisition, Investigation, Conceptualization, Methodology, Writing – review & editing. **A.N. Olimov:** Resources, Data curation, Formal analysis, Investigation, Visualization, Resources, Conceptualization, Methodology, Writing – review & editing. **R. Khurramov:** Resources, Data curation, Formal analysis, Investigation, Conceptualization, Methodology, Writing – review & editing. **D.Z. Isakov:** Investigation, Conceptualization, Methodology, Writing – review & editing. **M. Pirimmatov:** Investigation, Conceptualization,

Table 3
Observed Raman modes of Sb_2Se_3 films deposited at different source temperatures.

Observed Raman modes												Published data					
T_{source}=830 °C		T_{source}=840 °C		T_{source}=900 °C		T_{source}=975 °C		T_{source}=980 °C		T_{source}=1000 °C		Sb_2Se_3 [25,26,29]	Se_n (spiral chains) [28,29]	Se_6, Red Se* (rings) [28]	α, β –Sb_2O_3 [25,27,30]	Sb [25,26]	
Peak position, cm^{-1}	FWHM, cm^{-1}	Peak position, cm^{-1}	FWHM, cm^{-1}	Peak position, cm^{-1}	FWHM, cm^{-1}	Peak position, cm^{-1}	FWHM, cm^{-1}	Peak position, cm^{-1}	FWHM, cm^{-1}	Peak position, cm^{-1}	FWHM, cm^{-1}	Peak position, cm^{-1}	Peak position, cm^{-1}	Peak position, cm^{-1}	Peak position, cm^{-1}	Peak position, cm^{-1}	
80	23	85	26	80	19	80	20	80	14	77	15	80					
101	25	102	21	99	11	102	17	102	11	102	25			102			
		110	8	110	16			110	17	110	10					110	
117	20					118	24			118	9				118		
123	33	122	29	123	36	123	21			125	10			129	123		
						129	21	129	42	131	10				140		
								139	11	139	15					151	
153	31	153	27	153	14	153	23	153	10	153	27	151					
190	21	190	17	190	17	188	20	185	21	187	35	189			189		
208	8	212	8	208	6	212	6	209	7	209	13	210					
233	84	235	11			238	7	235	9				234–237				
						251	186			254	60	257		250*		255	

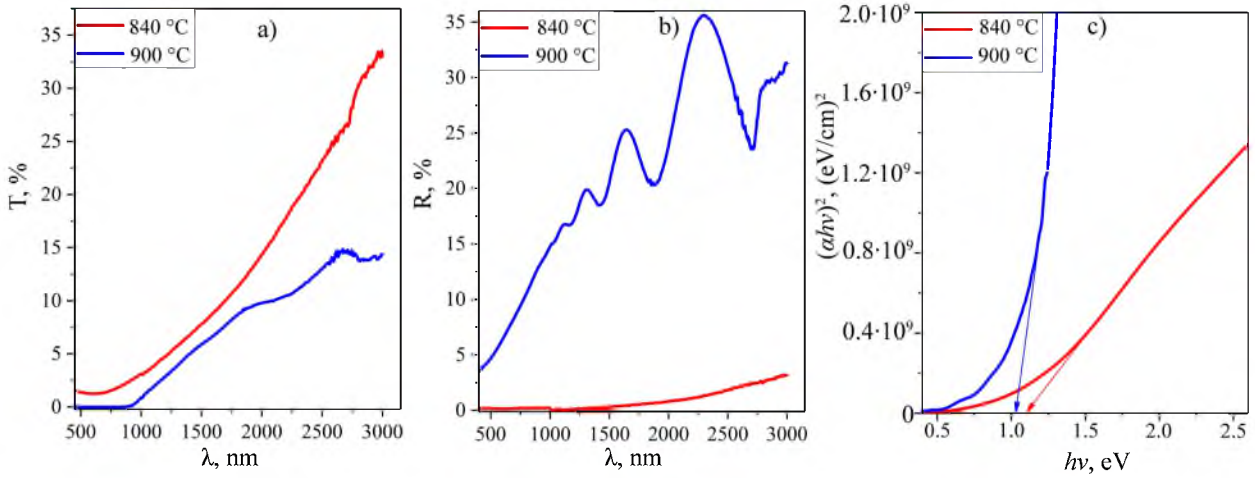

Fig. 9. (a) Transmission and (b) Reflection spectra, (c) Plots of function $(\alpha h\nu)^2 = f(h\nu)$ for Sb_2Se_3 films obtained at T_{source}=900 °C (E_g=1.04 eV) and T_{source}=840° C (E_g=1.12 eV).

Table 4
Conductivity type and conductivity of samples obtained at different source temperatures of the Sb_2Se_3 binary compound.

T_{source}, °C	830	840	900	980	1000
Sb/Se	0.72	0.66	0.88	0.88	0.81
Conductivity type	p	p	n	n	n
Conductivity $(Ohm\cdot cm)^{-1}$, at 300 K	$3.13\cdot10^{-5}$	$1.03\cdot10^{-5}$	$4.13\cdot10^{-5}$	$2.87\cdot10^{-5}$	$2.38\cdot10^{-5}$

Methodology, Writing – review & editing.

Declaration of Competing Interest

The authors declare that they have no known competing financial interests or personal relationships that could have appeared to influence the work reported in this paper.

Data availability

The data that support the findings of this study are available from the corresponding author upon reasonable request.

Acknowledgments

This work was supported by the Ministry of innovative development of the Republic of Uzbekistan (Grant No: MRB-2021–540) and the State Committee on Science and Technology of the Republic of Belarus (Grant No: F21UZBG-022).

References

[1] X. Wang, R. Tang, C. Wu, C. Zhu, T. Chen, Development of antimony sulfide-selenide $Sb_2(S,Se)_3$ -based solar cells, J. Energy Chem. 27 (2018) 713–721, https://doi.org/10.1016/j.jechem.2017.09.031.
[2] P.K. N.air, G.V. G.arcía, E.A.Z. Medina, L.G. M.artínez, O.L. C.astrejón, J.M. O.rtiz, M.T.S. Nair, Antimony sulfide-selenide thin film solar cells produced from stibnite mineral, Thin Solid Films 645 (2017) 305–311, https://doi.org/10.1016/j.tsf.2017.11.004.
[3] A. Mavlonov, T. Razykov, F. Raziq, J. Gan, J. Chantana, Y. Kawano, T. Nishimura, H. Wei, A. Zakutayev, T. Minemoto, X. Zu, S. Li, L. Qiao, A review of Sb_2Se_3 photovoltaic absorber materials and thin-film solar cells, Sol. Energy 201 (2020), https://doi.org/10.1016/j.solener.2020.03.009.
[4] Y. Zhou, L. Wang, S. Chen, S. Qin, X. Liu, J. Chen, D.J. Xue, M. Luo, Y. Cao, Y. Cheng, E.H. Sargent, J. Tang, Thin-film Sb_2Se_3 photovoltaics with oriented one-dimensional ribbons and benign grain boundaries, Nat. Photonics. 9 (6) (2015) 409–415, https://doi.org/10.1038/nphoton.2015.78.
[5] X. Liu, J. Chen, M. Luo, M. Leng, Z. Xia, Y. Zhou, S. Qin, D.J. Xue, L. Lv, H. Huang, D. Niu, J. Tang, Thermal evaporation and characterization of Sb_2Se_3 thin film for substrate Sb_2Se_3/CdS solar cells, ACS Appl. Mater. Interfaces 6 (2014) 10687, https://doi.org/10.1021/am502427s.
[6] X. Liu, X. Xiao, Y. Yang, D.J. Xue, D.B. Li, C. Chen, S. Lu, L. Gao, Y. He, M.C. Beard, G. Wang, Sh. Chen, J. tang, Enhanced Sb_2Se_3 solar cell performance through theory-guided defect control, Prog. Photovolt. 25 (10) (2017) 861–870, https://doi.org/10.1002/pip.2900.
[7] Z. Li, X. Liang, G. Li, H. Liu, H. Zhang, J. Guo, J. Chen, K. Shen, X. San, W. Yu, E. I. Ruud Schropp, Y. Mai, 9.2%-efficient core-shell structured antimony selenide nanorod array solar cells, Nat. Commun. 10 (1) (2019) 125, https://doi.org/10.1038/s41467-018-07903-6. –125.
[8] Y.H. Kwon, Y.B. Kim, M. Jeong, H.W. Do, H.K. Cho, J.Y. Lee, Crystal growth direction-controlled antimony selenide thin film absorbers produced using an electrochemical approach and intermediate thermal treatment, Sol. Energy Mater. Sol. Cells. 172 (2017), https://doi.org/10.1016/j.solmat.2017.07.004.
[9] H.M. Pathan, C.D. Lokhande, Deposition of metal chalcogenide thin films by successive ionic layer adsorption and reaction (SILAR) method, Bull. Mater. Sci. 27 (2004), https://doi.org/10.1007/BF02708491.
[10] S.L. Benjamin, C.H. De Groot, A.L. Hector, R. Huang, E. Koukharenko, W. Levason, G. Reid, Chemical vapour deposition of antimony chalcogenides with positional and orientational control: precursor design and substrate selectivity, J. Mater. Chem. C 3 (2015), https://doi.org/10.1039/c4tc02327g.
[11] Y. Zhou, M. Leng, Z. Xia, J. Zhong, H. Song, X. Liu, B. Yang, J. Zhang, J. Chen, K. Zhou, J. Han, Y. Cheng, J. Tang, Solution-processed antimony selenide heterojunction solar cells, Adv. Energy Mater. 4 (2014), https://doi.org/10.1002/aenm.201301846.
[12] M.D. Khan, M. Aamir, M. Sohail, M. Sher, J. Akhtar, M.A. Malik, N. Revaprasadu, Novel single source precursor for synthesis of Sb2Se3 nanorods and deposition of thin films by AACVD: photo-electrochemical study for water reduction catalysis, Sol. Energy 169 (2018), https://doi.org/10.1016/j.solener.2018.05.026.
[13] F.I. Mustafa, S. Gupta, N. Goyal, S.K. Tripathi, Effect of temperature on the optical parameter of amorphous Sb-Se thin films, J. Optoelectron. Adv. Mater. 11 (2009).
[14] X. Liu, X. Xiao, Y. Yang, D.J. Xue, D.B. Li, C. Chen, S. Lu, L. Gao, Y. He, M.C. Beard, G. Wang, S. Chen, J. Tang, Enhanced Sb_2Se_3 solar cell performance through theory-guided defect control, Prog. Photovolt. Res. Appl. 25 (2017), https://doi.org/10.1002/pip.2900.
[15] L. Wang, D.B. Li, K. Li, C. Chen, H.X. Deng, L. Gao, Y. Zhao, F. Jiang, L. Li, F. Huang, Y. He, H. Song, G. Niu, J. Tang, STable 6%-efficient Sb_2Se_3 solar cells with a ZnO buffer layer, Nat. Energy 2 (2017), https://doi.org/10.1038/nenergy.2017.46.
[16] X. Wen, C. Chen, S. Lu, K. Li, R. Kondrotas, Y. Zhao, W. Chen, L. Gao, C. Wang, J. Zhang, G. Niu, J. Tang, Vapor transport deposition of antimony selenide thin film solar cells with 7.6% efficiency, Nat. Commun. 9 (2018), https://doi.org/10.1038/s41467-018-04634-6.

[17] G.X. Liang, X.H. Zhang, H.L. Ma, J.G. Hu, B. Fan, Z.K. Luo, Z.H. Zheng, J.T. Luo, P. Fan, Facile preparation and enhanced photoelectrical performance of Sb_2Se_3 nano-rods by magnetron sputtering deposition, Sol. Energy Mater. Sol. Cells. 160 (2017), https://doi.org/10.1016/j.solmat.2019.110154.

[18] D.B. Li, X. Yin, C.R. Grice, L. Guan, Z. Song, C. Wang, C. Chen, K. Li, A.J. Cimaroli, R.A. Awni, D. Zhao, H. Song, W. Tang, Y. Yan, J. Tang, Stable and efficient CdS/Sb_2Se_3 solar cells prepared by scalable close space sublimation, Nano Energy 49 (2018), https://doi.org/10.1016/j.nanoen.2018.04.044.

[19] F. Pattini a, S. Rampino, F. Mezzadri, D. Calestani, G. Spaggiari, M. Sidoli, D. Delmonte, A. Sala, E. Gilioli, M. Mazzer, Role of the substrates in the ribbon orientation of Sb2Se3 films grown by low-temperature pulsed electron deposition, Sol. Energy Mater. Sol. Cells 218 (2020), 110724, https://doi.org/10.1016/j.solmat.2020.110724.

[20] J. Zhou, H. Chen, X. Zhang, K. Chia, Y. Cai, Y. Caoa, J. Pang, Substrate dependence on (Sb4Se6)n ribbon orientations of antimony selenide thin films: morphology, carrier transport and photovoltaic performance, J. Alloys Compd. 862 (2021), 158703, https://doi.org/10.1016/j.jallcom.2021.158703.

[21] D. Wang, C. Song, X. Fu, X. Li, Growth of one-dimensional Sb2S3 and Sb2Se3 crystals with straw-tied-like architectures, J. Cryst. Growth 281 (2005) 611–615, https://doi.org/10.1016/j.jcrysgro.2005.04.064.

[22] V.L. Deringer, R.P. Stoffel, M. Wuttig, R. Dronskowski, Vibrational properties and bonding nature of Sb2Se3 and their implications for chalcogenide materials, Chem. Sci. 6 (2015) 5255–5262, https://doi.org/10.1039/c5sc00825e.

[23] T.M. Razykov, A.K. Shukurov, K.M. Kuchkarov, B.A. Ergashev, R.R. Khurramov, J. G. Bekmirzoyev, A.A. Mavlonov, Morphological and structural characteristics of sb_2se_3thin films fabricated by chemical molecular beam deposition, Appl. Sol. Energy 55 (2019) 376–379, https://doi.org/10.3103/S0003701X19060094.

[24] M. Wobst, Investigation of the Miscibility Gaps in the Binary Systems Silver-Tellurium, Indium-Tellurium, Gallium-Tellurium, Thallium-Tellurium and Antimony-Selenium,"*Scr,* Metall. 5 (1971) 583–585.

[25] P. Vidal-Fuentes, M. Guc, X. Alcobe, T. Jawhari, M. Placidi, A. Pérez-Rodríguez, E. Saucedo, V.I. Roca, Multiwavelength excitation Raman scattering study of Sb_2Se_3 compound: fundamental vibrational properties and secondary phases detection, 2d Mater. 6 (4) (2019), 045054, https://doi.org/10.1088/2053-1583/ab4029.

[26] A. Shongalova, M.R. C.orreia, B. Vermang, J.M.V. Cunha, P.M.P. Salomé, P.A. F. ernandes, On the identification of Sb_2Se_3 using Raman scattering, MRS Commun. 8 (2018) 865–870, https://doi.org/10.1557/mrc.2018.94.

[27] Z. Sui, S. Hu, H. Chen, C. Gao, H. Su, A. Rahman, R. Dai, Z. Wang, X. Zhengc, Z. Zhang, Laser effects on phase transition for cubic Sb_2O_3 microcrystals under high pressure, J. Mater. Chem. C 22 (2017) 5451–5457, https://doi.org/10.1039/C7TC01289F.

[28] A.K. Sinha, A.K. Sasmal, S.K. Mehetor, M. Pradhana, T. Pal, Evolution of amorphous selenium nanoballs in silicone oil and their solvent induced morphological transformation, ChemComm 50 (99) (2014) 15733–15736, https://doi.org/10.1039/C4CC08168D.

[29] K. Nagata, K. Ishibashi, Y. Miyamoto, Raman and Infrared Spectra of Rhombohedral Selenium, Jpn. J. Appl. Phys. 20 (1981) 463–469, https://doi.org/10.1143/JJAP.20.463.

[30] G. Mestl, P. Ruiz, B. Delmon, H. Knozinger, Sb_2O_3/Sb_2O_4 in reducing/oxidizing environments: an in situ Raman spectroscopy study, J. Phys. Chem. 98 (1994) 11276–11282, https://doi.org/10.1021/j100095a008.

[31] K. Yang, B. Li, G. Zeng, Effects of substrate temperature and SnO_2 high resistive layer on Sb_2Se_3 thin film solar cells prepared by pulsed laser deposition, Sol. Energy Mater. Sol. Cells 208 (2020), 110381, https://doi.org/10.1016/j.solmat.2019.110381.

[32] S. Li, H. Shen, J. Chen, et al., Effect of selenization temperature on the properties of Sb_2Se_3 thin films and solar cells by two-step method, J. Mater. Sci. Mater. Electron. 30 (2019) 19871–19879, https://doi.org/10.1007/s10854-019-02354-1.

[33] F. Haque, N. Kumar Elumalai, M. Wright, et al., Annealing induced microstructure engineering of antimony tri-selenide thin films, Mater. Res. Bull. 99 (2018) 232–238, https://doi.org/10.1016/j.materresbull.2017.11.014.